Pt-WO$_x$/C catalysts for α, β- unsaturated aldehydes hydrogenation: a NMR study of the effect of the reactant adsorption on activity and selectivity.

Marta Stucchi[1], Francesca Vasile[1], Stefano Cattaneo[1], Alessandro Vomeri[1], Ana B. Hungria[2] and Laura Prati*[1]

[1]Dipartimento di Chimica, Università degli Studi di Milano, Via Golgi 19, 20133, Milano, Italy.

[2]Departamento de Ciencia de los Materiales e Ingeniería Metalúrgica y Química Inorgánica, Facultad de Ciencias, Universidad de Cádiz, Campus Rio San Pedro, Puerto Real, 11510, Cádiz, Spain.

*corresponding author: laura.prati@unimi.it

Abstract

The selective hydrogenation of α,β-unsaturated aldehydes is an ideal case for studying the structure–activity relationships in heterogeneous catalysis. In particular, cinnamaldehyde can be used as probe molecule for revealing the competition between hydrogenation of C=C and C=O bond. Here, we investigated the effect of the modification of some Pt supported on carbon catalysts by WO$_x$ species in cinnamaldehyde hydrogenation as WO$_x$ species are reported to increase the adsorption and activation of the C=O group of α, β-unsaturated aldehydes. Classical techniques used for correlating the catalyst activity and the selectivity to the characteristic of the materials (XRD, HAADF-STEM, XEDS mapping and XPS) have been coupled with NMR relaxometry, as innovative application, to disclose how the molecule approaches the catalyst surface. This indeed constitutes a crucial aspect that rule the catalytic activity. Therefore, an innovative, holistic approach have been used to consider the whole catalytic system.

1. Introduction

Selective hydrogenation of unsaturated oxygenates is still a challenge that involves the need to continue the study and the development of new catalysts [1]. The major concern in developing new catalytic processes is mostly related to control the selectivity. The unsaturated alcohols are not the most thermodynamically favoured and, accordingly, with the common monometallic catalysts the hydrogenation of the C=C bond is more easily obtained over the hydrogenation of the C=O bond [2][3]. The selective hydrogenation of α,β-unsaturated aldehydes is an ideal case for the study of structure–activity relationships in heterogeneous catalysis [4], and, among various α,β-unsaturated aldehydes, cinnamaldehyde (CAL) is a presentative probe molecule for revealing the competition between hydrogenation of C=C and C=O bond [5]. Both products of hydrogenation, i.e. hydrocinnamaldehyde (HCAL) and cinnamyl alcohol (COL), are useful intermediates in

pharmaceuticals and perfumery [6]. Further hydrogenation results in hydrocinnamyl alcohol (HCOL) and phenyl propane (PPR) by hydrogenolysis (Fig. 1) [7].
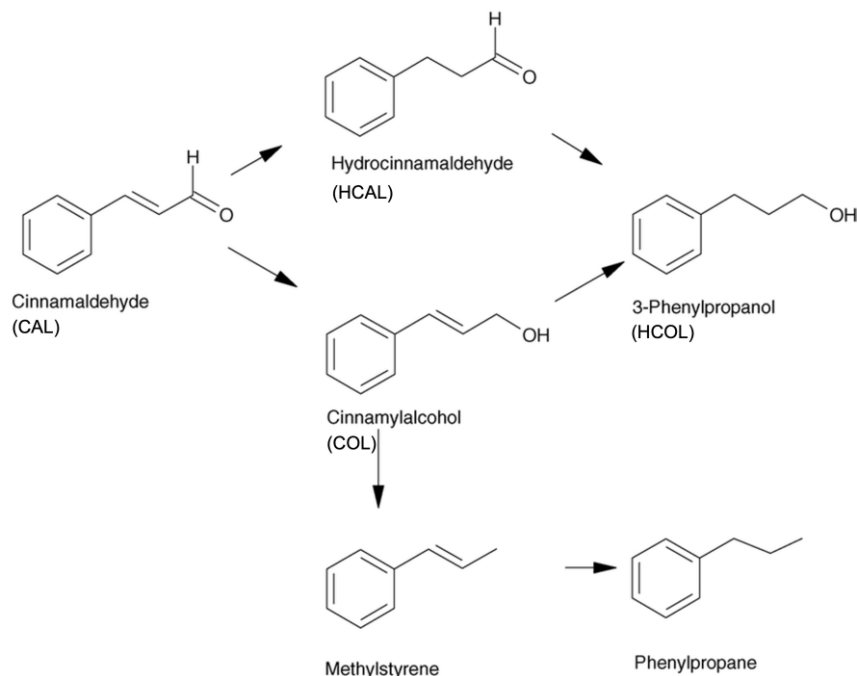

Fig. 1 Possible pathways for cinnamaldehyde hydrogenation.

Pt is known as one of the most active catalyst for hydrogenation/hydrogenolysis and it was extensively investigated for aldehydes hydrogenations. In particular, it has a potential high activity for the selective hydrogenation of C=O due to its large d band, which leads to the strongly repulsive four-electron interaction with the C=C bond and strongly attractive interaction with the C=O bond [8]. However, it is still too expensive as always happens in the case of noble metals [9]. The combination of Pt with a second metal could reduce the amount of Pt needed to have a worthy activity, but also be beneficial for directing the selectivity [10].

It was reported that the selectivity of hydrogenation reaction mainly depends on the adsorption of the substrate on the metal surface [11]. Surface science studies have also suggested that the modification of the metal-support surfaces can be used to tune the adsorption geometry and to alter the electronic structure through charge transfer, which contributes to the improvement of selectivity in hydrogenation of α, β-unsaturated aldehyde [12] [13][14].

The modification of the catalyst surfaces can be done adding a second metal or metal-oxide compound [15]. For example, Qin et al. [12] recently reported the synergistic effects between CoO_x and Pt in CoO_x-Pt/TiO_2 catalysts in the hydrogenation of cinnamaldehyde: the ~~bimetallic~~ catalyst containing two metal species showed higher selectivity to cinnamyl alcohol than the monometallic, ascribed to the increased oxygen vacancy resulting from the promoted hydrogen spillover. Hu at al.

[16] showed that FeO$_x$@Pt interface structure enhanced the C=O selectivity from 47 to 84% in cinnamaldehyde hydrogenation compared to the monometallic reference Pt/Al$_2$O$_3$, due in this case to the electron transfer from Fe to Pt and steric hindrance effect by FeOx.

Here, we investigated the effect of the modification of some Pt supported on carbon catalysts by WO$_x$ species. Indeed, WO$_3$ has highly electron-deficient sites that can increase the adsorption and activation of the C=O group of α, β-unsaturated aldehydes [17], as well as WO$_3$ species can generate different acidic sites which should affect the selectivity [18][19]. For example, Chary et al. [19] studied the influence of WO$_3$ loading on the conversion of levulinic acid over Pt–WO$_3$/γ-Al$_2$O$_3$ and they found a strong correlation between the W content with activity and selectivity of the reaction. The greater catalytic performance of the catalyst was attributed to the enhanced acidity due to the incorporation of tungsten oxide, high surface area, greater dispersion of Pt and the synergistic interaction between active species and the support.

In this work Pt/C was modified by WO$_x$ using different approaches, resulting in different chemical and physical surface properties. The different activity and selectivity were conventionally correlated to the physical-chemical characteristic of the materials through XRD, HAADF-STEM, XEDS mapping and XPS characterization, but also by the whole system point of view using NMR relaxometry, recently reported as an innovative technique to study the effect of the reactant adsorption in the presence of a solvent on activity and selectivity [20].

The adsorption/desorption of the reactant (R) and the product (P), as well as diffusion to the active site, are all important factors which determine the activity of a catalyst. Too weak adsorption often results in low catalytic activity, whereas a too strong interaction could result in irreversible adsorption and consequent deactivation of the active site. Furthermore, the presence of a solvent can have a significant impact on the adsorption step. Nuclear Magnetic Resonance spectroscopy has recently been shown to be a useful tool for determining the extent of interaction between the reactant and the catalyst in the present of solvent [21][22][23]. Spin relaxation can be considered a sensitive probe for molecular dynamics as the relaxation times like T1 (longitudinal) and T2 (transverse) may be employed to detect molecular dynamics processes [24]. In particular, ^{13}C NMR relaxation was successfully applied to study the role of the reactant structure effect in aldehydes hydrogenation using carbon based catalysts [20], where the large chemical shift range of ^{13}C allows for the discrimination of individual resonances and the measurement of the interaction of each individual carbon atom with the catalyst surface. In particular, the T1$_{ads}$/T1$_{bulk}$ ratio is used as an adsorption strength signal, where the T1$_{ads}$ is the relaxation time for the surface adsorbed (ads) molecule and the T1$_{bulk}$ is the relaxation time for the free diffusing (bulk) molecule. The lower the T1$_{ads}$/T1$_{bulk}$ ratio the higher the adsorption strength, which allows a direct correlation with catalyst performance.

2. Experimental

2.1 Materials and methods

The carbon used as catalytic support was Activated Charcoal Norit from Sigma-Aldrich. For the preparation of the WO_x/C modified supports, $Na_2WO_4 \cdot 2H_2O$ (ACS reagent, ≥99%, Sigma Aldrich) was used as precursor. For the synthesis of Pt nanoparticles, Sodium tetrachloroplatinate(II) (Na_2PtCl_4, Sigma Aldrich) was used as precursor, sodium borohydride ($NaBH_4$, Sigma Aldrich) was used as reducing agent and Polyvinyl alcohol (PVA, M_w 13,000-23,000, 87-89% hydrolysed solution, Sigma Aldrich) was used as protecting agent.

2.1.2 *Synthesis*

1% Pt supported on carbon was prepared by sol-immobilisation. Briefly, in 100 ml of milli-Q water, 1 mL of Pt(II) solution (10 mg/ml) was added under stirring, followed by PVA (having a Pt:PVA molar ratio of 2:1). $NaBH_4$ was then added fast keeping the solution under stirring to reduce Pt(II) (having a $NaBH_4$/Pt molar ratio of 8:1). After 30 min, 1 g of the carbon support was added with drops of sulphuric acid to keep the solution at pH 2. After 3 h of continuous stirring, the suspension was filtered and dried at 80 °C.

The monometallic Pt/C was firstly modified adding WO_3. Tungsten oxides either in the form of sol, gel or particles, were typically prepared via hydrolysis of the tungstate salts [25]. So, the previously synthesized 1%Pt/C catalyst was suspended in an aqueous solution of Na_2WO_4 (calculating the amount of Na_2WO_4 to have a theoretical W loading of 10% wt.). The suspension was stirred for 30 minutes at room temperature (RT), then 2 ml of a HCl aqueous solution were added dropwise to form WO_3 ($Na_2WO_4 + 2HCl + H_2O \rightarrow WO_3 \cdot 2H_2O + 2NaCl$). To prepare the 2 ml of HCl solution, 100 µL of HCl 37% wt. were added to 2 ml of milli-Q water (W:HCl molar ratio of 0.5). After 24 h of stirring, the slurry was filtered, washed several times, and dried at 80 °C.

A second series of W-modified carbon catalysts were prepared by a different methodology to investigate the impact of preparation on W oxidation state. In particular, the effect of temperature on oxide formation was investigated. Carbon was impregnated by Na_2WO_4, suspending the carbon powder in the aqueous solution of Na_2WO_4 (calculating the amount of Na_2WO_4 to have a theoretical W loading of 10% wt.). Then, the powders were calcined under N_2 atmosphere for 5 h at 400°C or 550°C (thus obtaining the first two samples labelled as WO_x/C_400 and WO_x/C_550).

Pt NPs were then supported on these two WO_x/C samples. Pt NPs were added both by impregnation-reduction or sol-immobilization method, in order to compare possible differences derived from different synthesis methodology. In the case of impregnation-reduction, Na_2PtCl_4 was used as precursor and $NaBH_4$ as reducing agent. 1 mL of a Na_2PtCl_4 solution (10 mg ml^{-1}) was diluted in 50 mL of milli-Q water, then 1 g of WO_x/C powder was added in the solution under continuous stirring.

After 2 h of continuous stirring at RT the powder was filtered and washed with distilled water; then, it was suspended again in 50 mL of water for the reduction of Pt by $NaBH_4$, added directly under stirring ($NaBH_4$:metal molar ratio of 8:1). After 1 h, the catalyst was filtered, washed, and dried at 80 °C for 2 h.

In the case of sol-immobilization, 1 mL of the Na_2PtCl_4 solution (10 mg ml⁻1) was added to 100 ml of milli-Q water under stirring, followed by PVA (Pt:PVA molar ratio of 2:1). Then, $NaBH_4$ was added fast keeping the solution under stirring ($NaBH_4$/Pt molar ratio of 8:1). After 30 min, 1 g of the WO_x/C powder was added and after 3 h of continuous stirring, the suspension was filtered and dried at 80 °C.

Table 1 reported the whole list of the catalyst obtained.

Table 1. Sample list

Sample label	Synthesis
Pt/C	Pt by Sol-immobilization (precursor: Na_2PtCl_4)
Pt-WO_x/C(400)_Sol	Pt by sol-immobilisation on WO_x/C_400
Pt-WO_x/C(400)_Imp	Pt by impregnation-reduction on WO_x/C_400
Pt-WO_x/C(550)_Sol	Pt by sol-immobilisation on WO_x/C_550
Pt-WO_x/C(550)_Imp	Pt by impregnation-reduction on WO_x/C_550
Pt-WO_3/C_HCl	Pt by sol-immobilisation, addition of WO_3 by acidic precipitation using HCl

2.2 Characterization analyses

XRD analyses were performed by a Miniflex 600-Rigaku X-ray diffraction (XRD) equipment (Panalytical S.R.L., Milan, Italy), using monochromatic Cu Kα radiation (λ = 1.5405 Å) and operating at 40 kV and 15 mA (2θ range of 5–80°).

Transmission electron microscopy (TEM) was performed with a TEM/STEM FEI Talos F200X G2 microscope, equipped with 4 Super-X SDDs. HAADF-STEM images and XEDS maps were acquired using a high brightness electron probe in combination with a highly stable stage which minimized sample drift.

X-ray photoelectron spectra (XPS) were acquired in an M-probe apparatus (Surface Science Instruments) (Thermofischer, Waltham, MA, USA) equipped with an atmospheric reaction chamber. The XPS lines were recorded by applying an Al Kα characteristic X-ray line, hv = 1486.6 eV. All data were analysed using ESCA Hawk software (Service physics Inc., Bend, OR, USA). The XPS lines of C 1s, O 1s, W 4f and Pt 4f were recorded.

2.2.1 NMR adsorption analyses

Chloroform-d (CDCl$_3$) has been purchased from Sigma-Aldrich and used as reference solvent considering that it is not adsorbed on carbon-based catalysts [26]. The NMR tube has been prepared adding ~15 mg of the catalyst and ~700 µL of cinnamaldehyde solution (in CDCl$_3$). The concentration of the aldehyde solution was set at 0.15 M as in the catalytic experiment.

NMR analyses were carried out on a Bruker Avance NEO 400 MHz spectrometer at 298 K. For compound characterisation and ^{13}C chemical shift identification, the J-modulated spin-echo sequence was used with 64k points in the time domain and 256 scans.

T1 measurements were obtained using standard inversion recovery from Bruker library (T1 measurements using inversion recovery with power gated decoupling).

For the T1 calculations it was assumed that the equilibrium is approached exponentially, and therefore the magnetisation along the z-axis is represented by Equation (1).

$$M_z = M_0(1 - e^{-t/T1}) \qquad (1)$$

M$_0$ is the magnetization at thermal equilibrium, t is the time elapsed, and T1 is the time constant obtained by plotting M$_z$ as a function of time. The pulse sequence used in the inversion-recovery experiment was:

d1 − p1(180°) − d2 − p2(90°) − FID

In this experiment, the nuclei are first allowed to relax to equilibrium. A 180° pulse (p1) is then applied to invert the signals. The signals are then allowed to relax for a length of time (d2) that is varied in each experiment. After the variable d2 (recovery delay), a 90° pulse (p2) was applied, and the FID was recorded. The FID records the spectrum intensity as a function of the variable delay d2. The signal will have relaxed more with longer d2. The peak intensity will reflect the extent to which each signal has relaxed during the d2 period.

14 T1 recovery delays were used ranging from 0.05 ms to 100 s. We used 8 repeat scans and a relaxation delay (d1) of 50 s between each scan to ensure a maximum signal (and to ensure the reach of the equilibrium, the d1 delay in the pulse sequence should be set to ~5 × the longest T1 of interest in the molecule) was maintained at all times.

The analysis of the T1 measurements was performed with the standard Bruker routine for T1/T2 calculation and with the Bruker Dynamic Center software version 2.5.6, using the following fitted function:

f(t) = I$_0$ × [1 − a × exp (−t/T1)]

where I$_0$ is the equilibrium magnetization and the parameter a determine the magnetization at time zero, that thus corresponds to I$_0$(1 − a).

2.3. Catalytic Reaction

Cinnamaldehyde hydrogenation has been carried out in a batch autoclave equipped with a glass inlet, at 80 °C and 5 bar of H_2. The amount of the catalyst was calculated in order to have a metal:substrate molar ratio equal to 1:1000. The starting concentration of CAL was 0.15 M in 2-propanol. GC analyses performed by a Thermo Scientific TRACE 1300 Instrument (Waltham, MA, USA) equipped with an Agilent HP-5 column gave CAL conversion and products formation over time, using undecane as an external standard. Sampling occurred at time 0 and every 30 min, until the end of the reaction. The quantification of products was performed by calibrating the response with authentic samples.

3. Results

3.1 Catalysts Characterization

XRD diffractograms of Pt/C, Pt-WO$_x$/C_400, Pt-WO$_x$/C _550 and Pt-WO$_3$/C_HCl catalysts are reported in Fig. 2. The XRD patterns of the Pt-WO$_x$/C_400 and Pt-WO$_x$/C _550 indicate both samples *sol.* and *imp.* (table 1) since they were superimposable.
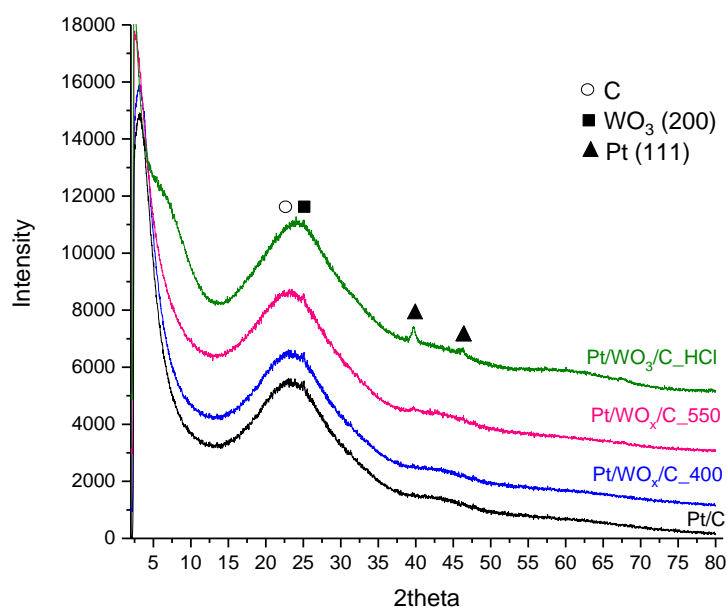

Fig. 2 XRD diffrattograms

The XRD pattern of the Pt/C showed a diffuse diffraction peak at around 21° which is typical of the amorphous carbon [27]. The diffractive peaks related to WO3 which should appear at 23-24° [28]

are covered by the diffuse peak of amorphous carbon. The 1 % wt. loading of Pt and a probably a very small Pt particle size could be the reasons why the diffraction peak related to Pt are not clearly detectable, except in the case of the Pt-WO$_3$/C_HCl, probably because of bigger Pt nanoparticles. In particular, the diffraction peaks at 39.9° and 46.0° correspond to the indexed planes (111) and (200) [29] [30], respectively.

The actual metal loading was measured by ICP-OES analyses (Table 2).

Table 2. Total metal content from ICP analyses.

Sample name	Pt % (wt)	W % (wt)	W/Pt
Pt/C	0.98	-	-
Pt-WO$_x$/C(400)_Sol	0.88	1.00	1.14
Pt-WO$_x$/C(400)_Imp	0.57	0.27	0.48
Pt-WO$_x$/C(550)_Sol	0.84	4.04	4.81
Pt-WO$_x$/C(550)_Imp	0.63	1.08	1.71
Pt-WO$_3$/C_HCl	0.98	5.01	5.27

In the case of monometallic Pt/C and in the case of the Pt/WO$_3$_HCl the loading of Pt was 0.98 % wt., nearly equivalent to the theoretical one (1% wt.). Differently, in the other Pt-WO$_x$/C catalysts the Pt loading was lower, depending on the method used for Pt NPs synthesis: by sol-immobilization we obtained a Pt loading of 0.88 % in the Pt-WO$_x$/C(400)_Sol, and of 0.84 % in the Pt-WO$_x$/C(550)_Sol; by impregnation we obtained an even lower Pt loading of 0.57% in the Pt-WO$_x$/C(400)_Imp and of 0.63% in the in the Pt-WO$_x$/C(550)_Imp.

Considering W, the actual loading calculated by ICP was always lower than the theoretical one (10 % wt.), but with large differences depending on the synthetic method used. The Pt/WO$_3$_HCl showed a W content of 5 % wt., followed by the Pt-WO$_x$/C(550)_Sol which showed a W content of 4 % wt.; then, the Pt-WO$_x$/C(550)_Imp showed a W content of about 1.00 wt. %, equal to that of Pt-WO$_x$/C(400)_sol; finally, in the Pt-WO$_x$/C(400)_Imp the amount of W was the lowest, of 0.27 %. Overall, the samples calcined at 550 °C showed higher Pt and W content compared to samples calcined at 400 °C. Moreover, the samples where Pt is added by impregnation-reduction showed a lower Pt loading and a W loading 4 times lower than samples by sol-immobilization. This result could be primarily ascribed to the different calcination temperature that could differently impact on the WO$_x$ interaction with C surface. Then, this different interaction could lead to the different detachment of W during the following step depending on Pt deposition technique. In particular we supposed that the treatment with NaBH$_4$ in the impregnation technique could promote the leaching of WO$_x$.

Further STEM characterization was performed on the bimetallic ~~samples~~ systems, to clarify the effect of different synthetic methods. Samples calcined at 550°C or at 400°C were compared considering the deposition of Pt NPs by sol-immobilization or impregnation-reduction (Fig. 3 and Fig. 5).

Considering the samples treated at 550°C (Fig. 3), Pt nanoparticles are clear visible and well dispersed on the carbon surface regardless the preparation method used (Fig. 3). There are always either some aggregation of Pt NPs about 20 nm in diameter or very small nanoparticles < 5 nm in diameter well dispersed on the support. W was detectable only in the Pt-WO$_x$/C(550)_sol, mostly deposited as an atomic dispersion on the carbon support (Fig. 4).
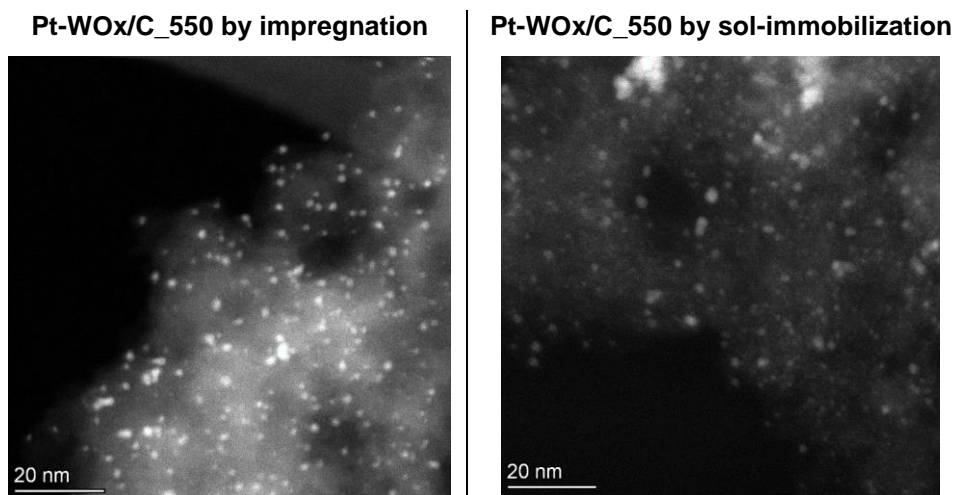
Pt-WOx/C_550 by impregnation | **Pt-WOx/C_550 by sol-immobilization**

Fig. 3 Representative HAADF-STEM images collected on Pt-WO$_x$/C_550 by impregnation (left side) and sol-immobilization (right side).
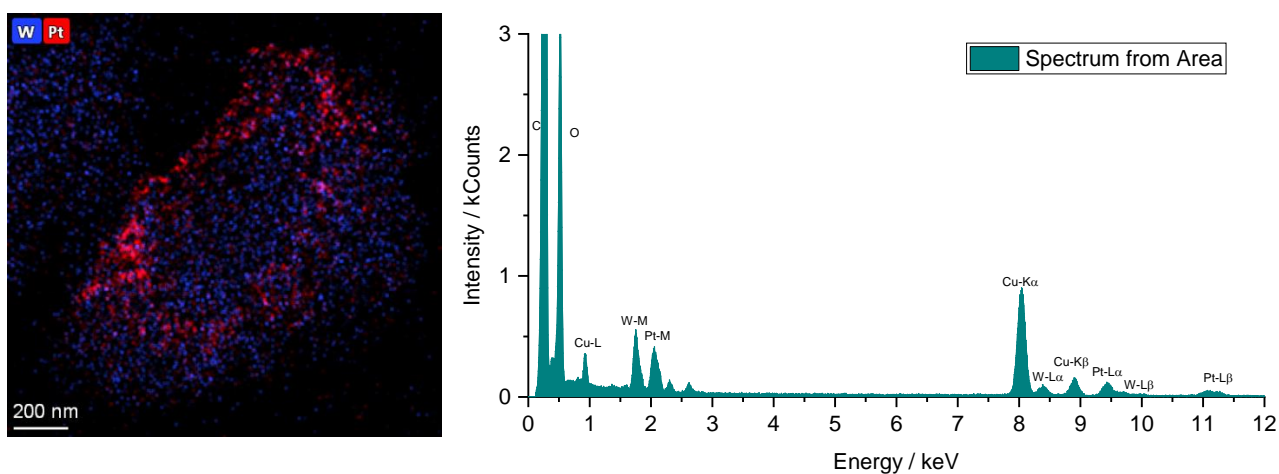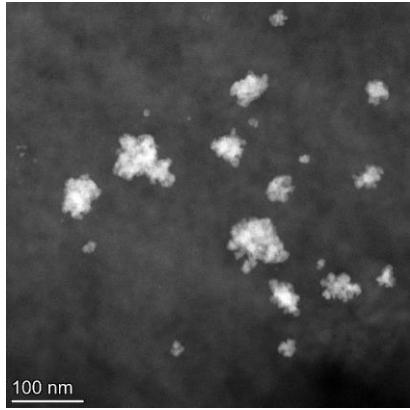

Fig. 4 XEDS mapping and spectrum of the entire area shown on the map of the 1%Pt-WOx/C_550(sol)

Considering the samples treated at 400°C, in the case of Pt-WO$_x$/C(400)_Imp HAADF-STEM images revealed Pt nanoparticles of big size (100-200 nm) randomly distributed on the carbon with a low dispersion (Fig. 5, left side). Otherwise, in the case of Pt-WO$_x$/C(400)_Sol the acquired images showed nanoparticles of 20-30 nm average size with a good dispersion (Fig. 5, right side). Also in this case, the W was detectable only in the sample prepared by sol-immobilization (see the XEDS maps at Fig. 6).

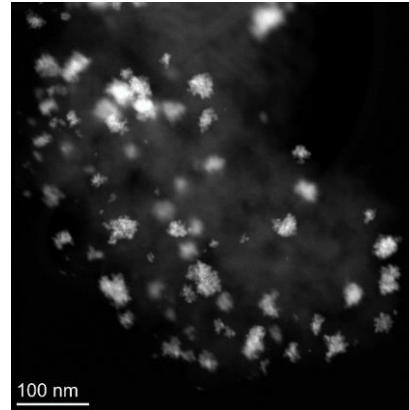**Pt-WOx/C_400 by impregnation** **Pt-WOx/C_400 by sol-immobilization**

Fig. 5 Representative HAADF-STEM images collected on Pt-WO$_x$/C_400 by impregnation (left side) and sol-immobilization (right side).
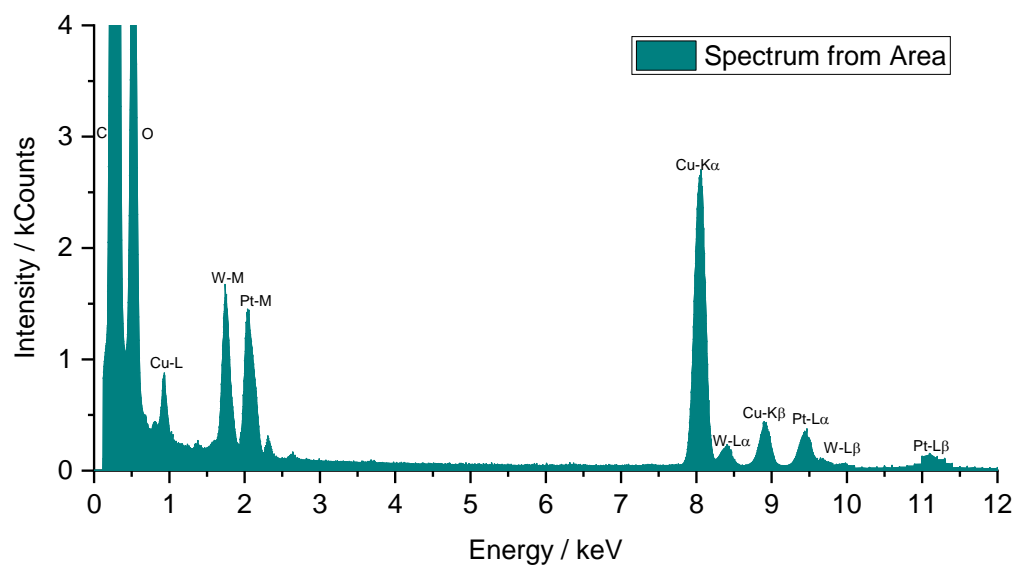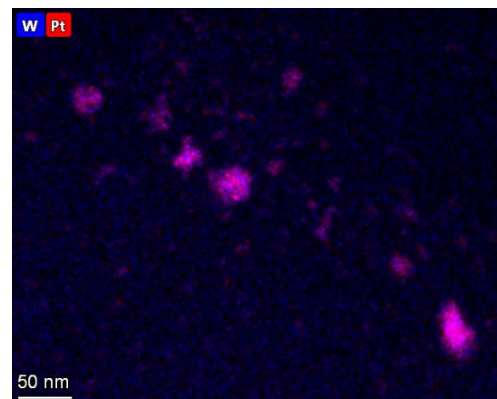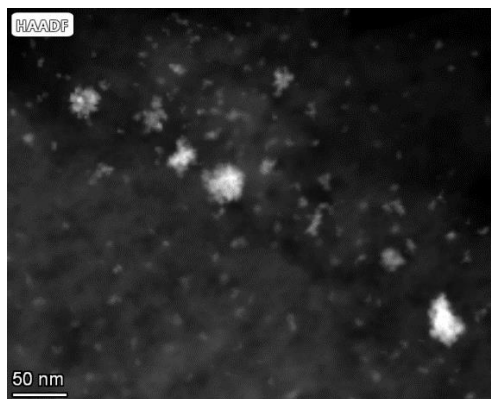

Fig. 6 HAADF-STEM images, XEDS mapping and spectrum of the entire area shown on the map of the 1%Pt-WO$_x$/C_400(sol)

Lastly, the HAADF-STEM and XEDS analyses were performed on the Pt-WO$_3$/C_HCl (Fig. 7). Pt NPs are mostly present as bigger agglomerates. This agrees with the XRD pattern of this sample (Fig. 2) which was the only one in which the peak of Pt was visible, that usually indicates the presence of bigger NPs.

W is also visible and well dispersed all over the carbon surface, as also revealed by the elemental maps (Fig. 8).
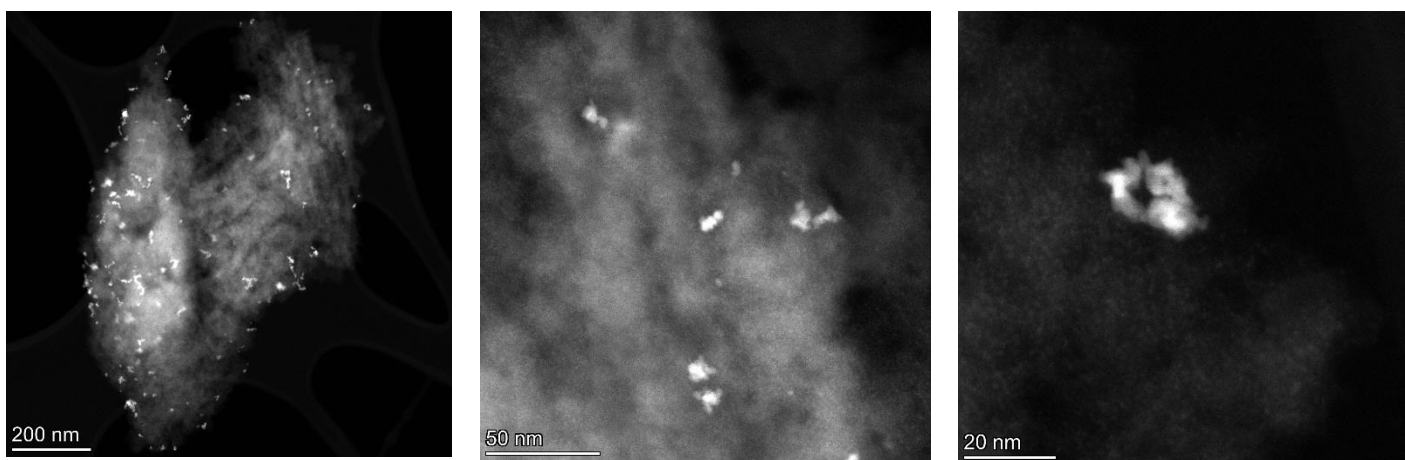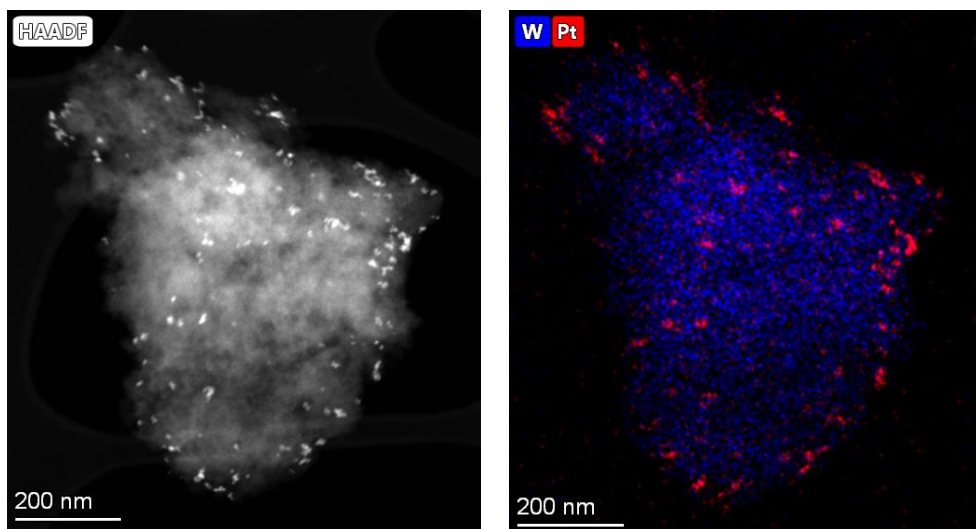

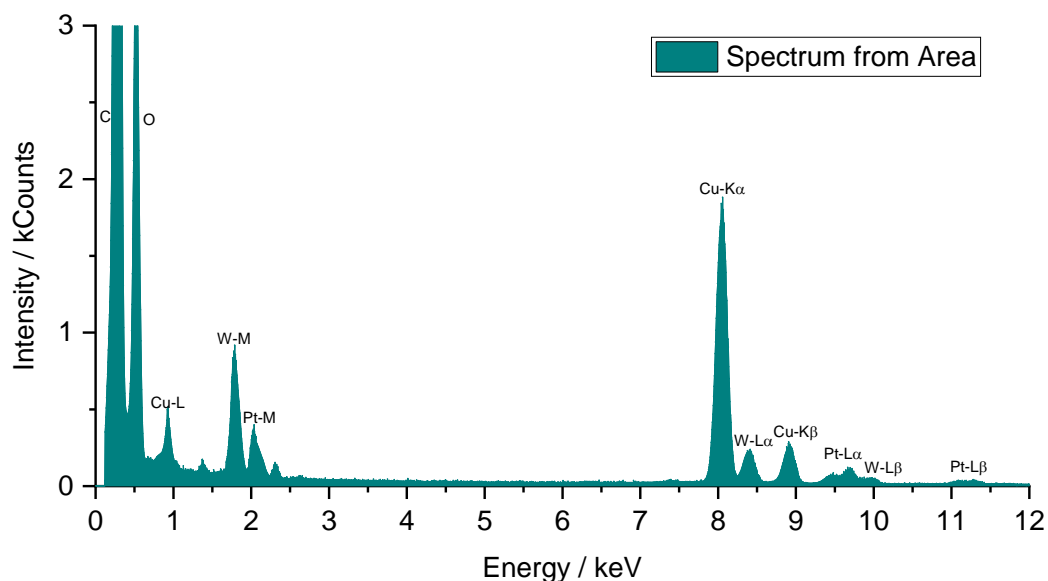**Fig. 7** Representative HAADF-STEM images collected on Pt-WO$_3$/C_HCl.

Fig. 8 HAADF-STEM image XEDS mapping and spectrum of the entire area shown on the map of the 1%Pt-WO₃/C_HCl

3.2 Catalysis

The activity and selectivity of the catalysts have been investigated towards the hydrogenation of cinnamaldehyde (CAL) (Fig. 9). We correlated the different physical-chemical properties to the catalytic behaviour with particular focus on the selectivity between C=C and C=O hydrogenation.

The reaction has been carried out in a batch autoclave equipped with a glass inlet, at 80 °C and 5 bar of H_2. The amount of the catalyst was calculated in order to have always a metal:substrate molar ratio equal to 1:1000. The starting concentration of CAL was 0.15 M in 2-propanol. The substrate conversion and products formation were evaluated by means of GC analyses over time, using undecane as an external standard. Sampling were withdrawn at 0, 15, 30, 60, 180, 240 and 300 minutes.

The cinnamaldehyde concentration over the time using the different catalysts is reported in Fig. 9. The initial activity is defined as the moles of cinnamaldehyde converted after 15 minutes of reaction, per mole of metal per min, and it can be evaluated from the initial part of the curves (Tab. 3).
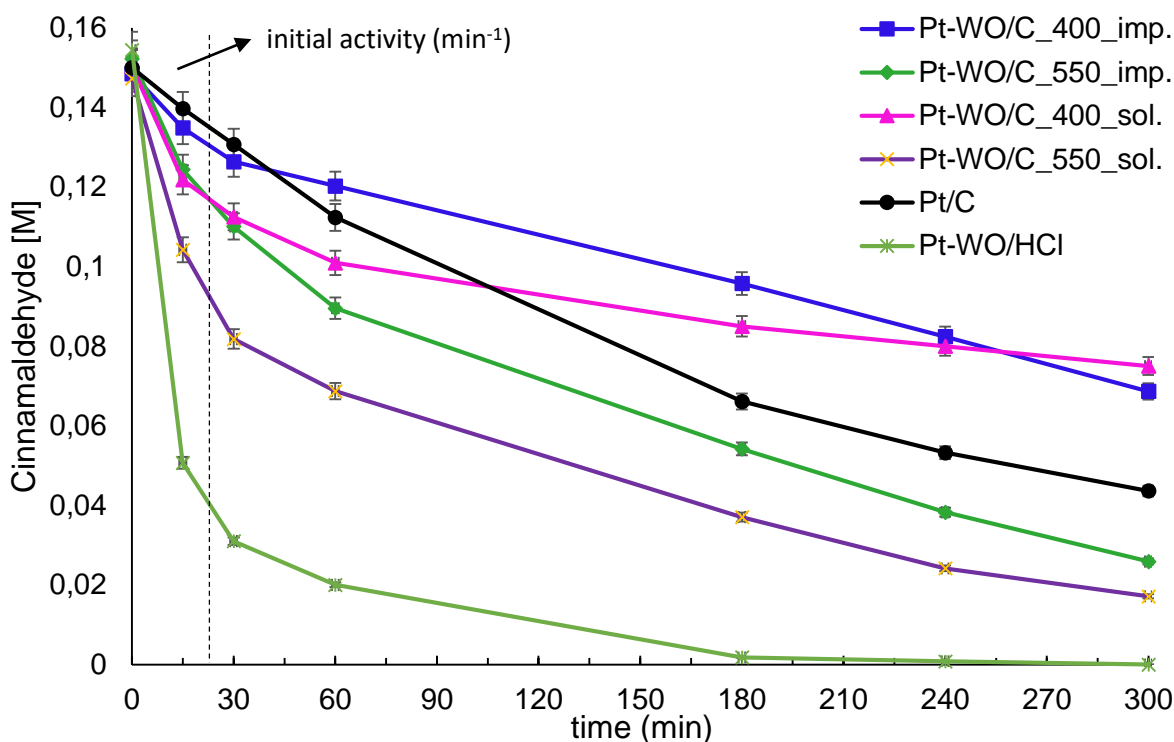
Fig. 9 Cinnamaldehyde concentration over time in cinnamaldehyde hydrogenation at 80 °C and 5 bar of H_2 using different Pt-WO-C catalysts.

Table 3. Initial activity of the catalysts defined as the moles of cinnamaldehyde converted after 15 minutes of reaction, per mole of metal per min.

Catalyst	Initial activity (min⁻¹)
Pt/C	444
Pt-WO$_x$/C(400)_Imp	622
Pt-WO$_x$/C(550)_Imp	1244
Pt-WO$_x$/C(400)_Sol	1289
Pt-WO$_x$/C(550)_Sol	1911
Pt-WO$_3$/C_HCl	4622

Comparing the activity of the monometallic Pt/C reference catalyst with the ~~catal bimetallic samples~~ bimetallic catalytic systems, the modification with WO$_x$ has a positive effect when the heating treatment was performed at 550 °C, whereas a negative one when the heating was performed at 400 °C (Fig. 9). Moreover, the synthesis of Pt by sol-immobilization resulted in a more active catalyst compared to the synthesis by impregnation-reduction. To be noted that, as clearly noted following the reaction profiles, that the catalysts derived from the 400°C thermal treatment underwent to deactivation.

The W/Pt ratio from ICP (Table 2) seems to be rather correlated to the initial activity: indeed, the less active catalyst Pt-WO$_x$/C(400)_Imp showed the lowest W/Pt ratio (0.48), while the most active Pt-WO$_3$/C_HCl showed the highest W/Pt ratio of 5.27. This conclusion could be supported also from

the comparison between the Pt-WO$_x$/C(400)_Sol and Pt-WO$_x$/C(550)_Imp, which showed comparable initial activity and very similar W/Pt ratio (1.14 and 1.71 respectively).

On the other hand, the lower activities of the samples calcined at 400 °C compared with those calcined at 550 °C can be explained looking at the STEM-XEDS analyses (Fig. 3-6). which highlighted a different Pt dispersion, that is very low in the samples treated at 400 °C compared with those treated at 550°C. The calcination at high temperature in fact seems to favour a better Pt dispersion.

Cinnamaldehyde hydrogenation can proceed through the hydrogenation of the C=C bond, forming first hydrocinnamaldehyde (HCAL), or through the hydrogenation of the C=O bond, forming cinnamyl alcohol (COL). After further hydrogenation steps, also 3-phenyl propanol (HCOL), methyl styrene, and phenyl propane can be formed (Fig. 1).

The selectivity (measured at 50 % of conversion) of the catalysts is reported in Fig. 10. Samples treated at the same calcination temperature behaved similarly in terms of selectivity.
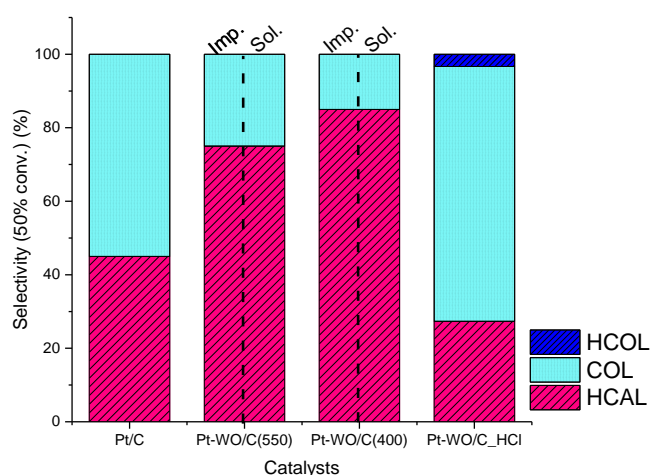

Fig. 10 Selectivity at 50% conversion obtained with different Pt-based catalyst towards cinnamaldehyde hydrogenation.

The monometallic catalyst Pt/C which showed an initial activity of 444 min^{-1} converted cinnamaldehyde to hydrocinnamaldehyde (HCAL) and cinnamyl alcohol (COL) with a selectivity at 50% conversion of 45 % and 53 % respectively (Fig. 10, 1st column). The bimetallic catalytic system ~~catalysts~~ Pt-WO$_x$/C(550) at the same conversion showed increased selectivity to HCAL (75 %) compared to the monometallic, which increased further (up to 85 %) in the case of Pt-WO$_x$/C(400) samples. On the contrary the Pt-WO$_3$/C_HCl showed a selectivity of only 27.3 % to HCAL, but 69.3 % to COL, and 3.3 % to HCOL, not observed in the other cases (Fig. 10). To be noted that, as indicated in Fig. 10, catalysts prepared by impregnation or sol-immobilization at the same calcination

temperature showed the same selectivity, despite their differences in terms of Pt dispersion and W/Pt ratio, parameters which apparently affected the activity of the catalysts.

Therefore, for disclosing the ruling factors of the different selectivity, we further investigate by XPS other characteristics of catalyst such as the metal exposure and the metal oxidation state, parameters well known to have an impact on catalysis.

3.3 XPS Analyses

We focused our attention of sol-prepared catalysts. XPS survey analyses (Tab. 4) showed a Pt atomic exposure of 0.28 % in the monometallic Pt/C, which is higher than that revealed in the case of bimetallic systems samples. In particular, bimetallic catalytic systems catalysts showed different Pt exposure depending on the method used for their synthesis, i.e. 0.25 % in the $Pt-WO_3/C$ and 0.06 % in both $Pt-WO_x/C(400)$ and (550). Likewise, they showed a different W exposure, which in the case of $Pt-WO_x/C(400)$ was so low to be under the detection level. The correlation of this parameter with catalytic activity confirmed the trend observed considering the ICP data: the higher the ratio Pt/W the higher the activity.

Table 4. XPS survey analysis.

Catalyst		W 4f	Pt 4f
Pt/C	B.E. (eV)	-	71.4
	At. %	-	0.28
Pt-WO$_x$/C(400)_sol	B.E. (eV)	nd	75.8
	At. %	nd	0.06
Pt-WO$_x$/C(550)_sol	B.E. (eV)	37.5	74.7
	At. %	0.08	0.06
Pt-WO$_3$/C_HCl	B.E. (eV)	36.5	74.4
	At. %	0.26	0.25

From the deconvolution of the Pt 4f signal (Tab. 5) we found both Pt^0 (B.E. 71.3 eV) and Pt^{2+} (B.E. 72.5 eV).

Table 5. XPS analysis from the deconvolution of high-resolution of Pt 4f.

	Pt 4f			
	Pt^0 (71.0 eV)		Pt^{II} (72.4 eV)	
	B.E. (eV)	At. %	B.E. (eV)	At. %
Pt/C	71.3	61.5	72.5	38.5
Pt-WOx/C(400)_sol	nd	nd	nd	nd
Pt-WOx/C(550)_sol	71.6	61.0	72.6	39.0
Pt-WO3/C_HCl	71.1	53.5	72.2	46.5

In the monometallic Pt/C, the relative amount of Pt^0 was higher than that of Pt^{2+}, 61.5 % and 38.5 % respectively, similar to that showed by the bimetallic system Pt-WO$_x$/C(550)_sol. The Pt 4f signal measured in the case of Pt-WO$_x$/C(400)_sol was too low to have a reliable deconvolution, but we can suppose a similar composition due to the same metallic sol used. In the case of Pt-WO$_3$/C_HCl, the amount of Pt^0 slightly decreased (53.5 %), but it is still higher than the amount of Pt^{2+}.

The small differences revealed in the Pt oxidation states, lead us to conclude this parameter plays a role (if any) similar in all the sample. Therefore, we looked at the high-resolution spectra of W 4f (Tab. 6).

Table 6. XPS analysis from the deconvolution of high-resolution of W 4f spectra.

| | W 4f | | | |
| | WO$_2$ (33.1 eV) | | WO$_3$ (36.1 eV) | |
	B.E. (eV)	At. %	*B.E. (eV)*	At. %
Pt-WO$_x$/C(400)_sol	*33.1*	60.6	*36.14*	39.4
Pt-WO$_x$/C(550)_sol	*33.3*	56.6	*36.14*	43.38
Pt-WO$_3$/C_HCl	*33.5*	48.2	*36.44*	51.8

The amount of the superficial WO$_2$ and WO$_3$ can be evaluated by deconvolution of the W 4f signal. Pt-WO$_x$/C(400)_sol showed the highest amount of WO$_2$ (60.6 %), followed by Pt-WO$_x$/C(550)_sol (56.6 %) and then Pt-WO$_3$/C_HCl (48.2 %); accordingly, the amount of WO$_3$ followed an opposite trend. The different composition in terms of WO$_2$ and WO$_3$ could be one of the first explanation of the different activity and selectivity showed by the catalysts toward C=C or C=O hydrogenation. The co-presence of Pt and WO$_3$ improves the hydrogen spillover [31], and the interaction between Pt and WO$_3$ (usually improved by a high Pt dispersion) increases the electron density of Pt, which lead to an increased adsorption of the C=O group [32]. Indeed, Pt-WO$_3$ interfaces can activate carbonyl bonds due to the creation of sites capable of adsorbing and activating the C=O group. On the other hand, WO$_2$ was reported as efficient catalyst for the hydrogenation of linear olefins [33]: DFT calculations demonstrated in particular that oxygen-deficient surface of WO$_2$ can activate H$_2$ very easily in kinetics and thermodynamics, differently from WO$_3$, where the adsorption of H$_2$ is unfavourable and the breaking of the H−H bond is kinetically unfeasible (to be noted that the calculated adsorption free energies of H$_2$ on WO$_2$ and on WO$_3$ are of -0.346 eV and +0.436 eV, respectively).

Therefore, the high amount of WO$_3$ in the Pt-WO$_3$/C_HCl could be the reason of the higher capability of this sample to hydrogenate the C=O bond compared to the other catalysts; on the contrary, the

higher amount of WO_2 in the Pt-WO_x/C(400)_sol and (500)_sol could explain the high selectivity to HCAL, where the hydrogenation of C=C bond is favoured over the C=O.

Since now we search the ruling factors just looking the catalyst but the whole catalytic system is by far more complex and involve also the reactant and the reaction medium. Therefore, we also used an innovative approach through NMR relaxation that is a technique able to establish the real interaction of the reactant with the catalyst in the actual reaction medium. Indeed, NMR relaxation can be used to disclose how the molecule approaches the catalyst surface, which is another crucial aspect that rule the catalytic activity.

3.4 NMR Analyses

NMR relaxation can be used to probe the interaction between an organic substrate and the surface of a catalyst [20]. In particular, from ^{13}C NMR relaxation spectra T1 relaxation times can be derived for each carbon atom of the molecule. The $T1_{bulk}$ is calculated from the spectrum acquired on the free molecule in a solvent (conventionally $CDCl_3$), while the $T1_{ads}$ is calculated from the spectrum acquired in the presence of the catalyst.

Therefore, NMR analyses and corresponding $T_{ads}/T1_{bulk}$ calculations were performed on cinnamaldehyde on the W modified Pt catalysts. The $T_{ads}/T1_{bulk}$ ratio has been used as indicator of the relative strength of surface interaction, where the lower the $T_{ads}/T1_{bulk}$ ratio the lower the mobility, meaning strong adsorption. In particular, a $T_{ads}/T1_{bulk}$ ratio equal or very close to 1 indicates that there is no interaction between the substrate and the catalysts, as well as $T_{ads}/T1_{bulk}$ values ≥ 0.9 indicate a very weak interaction. On the contrary, values lower than 0.9 indicates that there is an interaction, which is stronger the more the value decreases [20]. As the catalytic activity is strongly affected by the adsorption/desorption equilibrium of reactants and products on the catalyst surface [34], the determination of the interaction between the substrate with the catalytic surface in the real reaction medium is crucial. ^{13}C NMR could provide useful data that could be correlated with the catalytic activity.

In this work, the adsorption of cinnamaldehyde on Pt/C, Pt-WO_x/C(400)_sol, 1%Pt-WO_x/C(550)_sol and Pt-WO_3/C_HCl, was studied. T1 relaxation times were calculated for the free diffusing cinnamaldehyde in $CDCl_3$ ($T1_{bulk}$) and in the presence of the catalyst ($T1_{ads}$). All the 7 different signals related to each specific carbon atom of cinnamaldehyde were observed (Fig. 11). $T_{ads}/T1_{bulk}$ values are reported in Table 6.

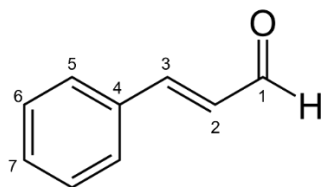**Fig. 11** Differentiation of cinnamaldehyde carbon atoms detectable by T1 ^{13}C NMR

Table 7. $T1_{ads}/T1_{bulk}$ ratio for all carbon atoms of cinnamaldehyde measured in presence of different catalysts. The value of this ratio is indicative of the interaction with the catalysts surface.

$T1_{ads}/T1_{bulk}$ #C	Pt/C	Pt-WO$_3$/C_HCl	Pt-WO$_x$/C(550)_sol	Pt-WO$_x$/C(400)_sol
1	0.50	0.85	0.79	0.96
2	0.67	0.88	0.90	1.03
3	0.43	0.85	0.66	0.83
4	0.82	0.97	0.92	1.03
5	0.67	0.97	0.87	0.96
6	0.64	0.96	0.88	0.92
7	0.69	0.97	0.88	0.98

Considering the monometallic Pt/C (1st column), the $T_{ads}/T1_{bulk}$ ratio values revealed a strong interaction ($T_{ads}/T1_{bulk}$ between 0.43 and 0.67).

For the analysis of the $T_{ads}/T1_{bulk}$ ratio of cinnamaldehyde interacting with the bimetallic catalytic systems, it is possible to observe some peculiar differences in the values of different carbons. From a selectivity point of view, it is useful to focus our attention on two different groups of carbon atoms: C_{1-3} and C_{4-7} (Fig. 12).
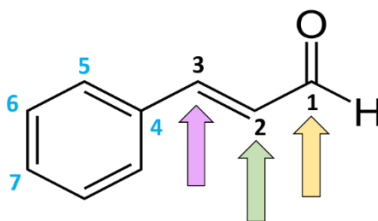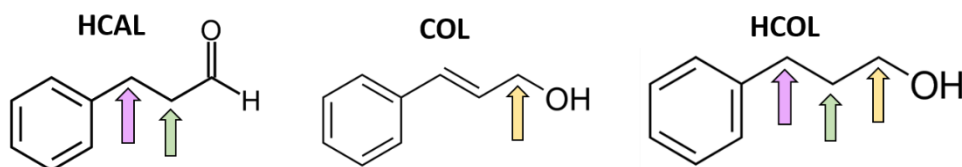
Fig. 12 The carbons of Cinnamaldehyde and its derivatives can be distinguished into two groups: the aromatic and the linear parts.

The first group could be used for determining the preferred orientation of C=C or C=O, while the second could be useful for determining the adsorption of the molecule through the aromatic ring. The differences observed between C_{1-3} and C_{4-7} values may suggest a selective adsorption of the carbon chain and of the carbonyl group of cinnamaldehyde rather than the aromatic ring, which resulted in a non-selective cinnamaldehyde conversion to the hydrogenation products, i.e. HCAL and COL (see Fig. 10 and Fig. 12).

In the Pt-WO$_3$/C_HCl, the values of C_{1-3} are lower than 0.9 (between 0.85 and 0.88), while the values of C_{4-7} are higher than 0.9., indicating that only the C_{1-3} atoms of the cinnamaldehyde interact with Pt-WO$_3$/C_HCl. To be note that the $T_{ads}/T1_{bulk}$ of C_1 (0.85) and that of C_{2-3} (0.86) are comparable, indicating a similar interaction of C=O and C=C.

Differently, in the Pt-WO$_x$/C(550)_sol the values of C_1, C_2 and C_3 differ the one from the other, with the lowest measured in the case of C_3 (0.66), followed by C_1 (0.79) and then C_2 (0.90). The values of C_{4-7} showed an average value of 0.88, suggesting an interaction of the aromatic ring with the catalyst.

Therefore, it seems that all the carbons of cinnamaldehyde are interacting with the catalyst with a not sharp separation between C_{1-3} and C_{4-7} values, which are lower than 0.9 in all cases: this is compatible with a flat molecule adsorption occupying different active sites, thus potentially reducing the activity of the catalyst. On the other hand, the difference between C_1 (0.79) and C_3 (0.66) suggests an enhanced interaction of the C=C double bond rather than the C=O, thus resulting in the higher selectivity toward HCAL then COL (Fig. 10).

Lastly, in the Pt-WO$_x$/C(400)_sol, the values of C_1 and C_2 higher than 0.9, as well as the values of C_{4-7} higher than 0.9, indicate a very low interaction, which can be in turn correlated to the low activity. However, the very selective adsorption of C_3 (0.83) compared to the other carbon atoms (>0.9) could be the reason of the high selectivity of this catalyst toward the C=C hydrogenation (Fig. 10).

To separate the contribution of C=C and C=O and disclose the fundamental role of the presence of C=C double bond in determining the interaction of CALD with the catalyst, we carried out some

further NMR measurements on HCAL, differentiating all the 7 signals related to each specific carbon atom (Fig. 13). $T_{ads}/T1_{bulk}$ ratio values for each carbon atom are reported in Table 8.
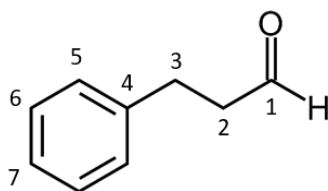

Fig. 13 Differentiation of hydrocinnamaldehyde (HCAL) carbon atoms detectable by T1 ^{13}C NMR.

Table 8. $T1_{ads}/T1_{bulk}$ ratio of each carbon atom of cinnamaldehyde measured during the interaction with the catalysts surface.

$T1_{ads}/T1_{bulk}$				
#C	Pt-WO$_3$/C_HCl	Pt-WO$_x$/C(550)_sol	Pt-WO$_x$/C(400)_sol	Pt/C
1	0.87	0.94	1.05	0.90
2	1.01	1.00	1.02	1.01
3	0.91	0.85	1.02	0.86
4	0.94	0.81	0.91	0.84
5	0.95	0.94	0.97	0.96
6	1.01	0.99	1.02	0.99
7	1.01	0.99	1.01	1.00

In this case it is clear that only in the case of Pt-WO$_3$/C_HCl it is possible to observe a $T1_{ads}/T1_{bulk}$ lower than 0.9 for C_1. Indeed, only this catalyst appeared to be able to produce the fully hydrogenated product (HCOL).

4. Conclusion

Five WO$_x$ modified Pt/C catalysts were obtained by differentiating the sequential addition of W precursors and Pt. Four samples were obtained by impregnating carbon with W precursor and then thermally treated at 400°C or 550°C; then Pt was added. On the contrary, the last sample was prepared by firstly added Pt followed by acidic deposition of WO$_x$. Of particular importance resulted the thermal treatment of WOx/C. Comparing the activity of the monometallic Pt/C with the bimetallic ~~samples~~ systems in the cinnamaldehyde hydrogenation, the modification with WO$_x$ had a positive effect and the activity can be correlated to the W/Pt ratio either calculated by ICP (bulk) or XPS (surface): the less active catalyst Pt-WO$_x$/C(400)_Imp showed the lowest W/Pt ratio (0.48), while the

most active Pt-WO₃/C_HCl showed the highest W/Pt ratio of 5.27. This conclusion could be supported also from the comparison between the Pt-WO$_x$/C(400)_Sol and Pt-WO$_x$/C(550)_Imp, which showed comparable initial activity and very similar W/Pt ratio (1.14 and 1.71 respectively).

Looking at the selectivity, the bimetallic catalytic system Pt-WO$_x$/C(550)_sol or imp and Pt-WO$_x$/C(400)_sol or imp showed increased selectivity toward C=C compared to the monometallic, while the Pt-WO₃/C_HCl showed an increased selectivity C=O. To be noted that the last catalyst is able to fully hydrogenate CAL to HCOL, not observed in the other cases. The amount of the superficial WO$_2$ and WO$_3$ evaluated by XPS gave a first explanation of this different selectivity. The high amount of WO$_3$ in the Pt-WO₃/C_HCl could be the reason of the higher capability of this sample to hydrogenate the C=O bond compared to the other catalysts. On the contrary, the higher amount of WO$_2$ in the Pt-WO$_x$/C(400)_sol and (500)_sol could explain the high selectivity to HCAL, where the hydrogenation of C=C bond is favoured over the C=O.

For a better understanding of the complex catalytic system constituted not only by the catalytic material but also by the reactant, the reaction medium etc. we use 13C-NMR relaxation times (T1bulk/T1ads) for establishing the real interaction of the reactant with the catalyst in the actual reaction medium. Focusing our attention on two different group of C (aromatic C1-C4 and aliphatic C1-C3) we found a direct correlation between the strength of reactant interaction and the catalytic surface with the reaction selectivity. In the Pt-WO₃/C_HCl, we found a stronger interaction of C1-C3 compared with those of the aromatic ring, with similar interaction of C=O and C=C situation that could be correlated with the ability of the catalyst to hydrogenate with similar rate both C=C and C=O. Accordingly this catalyst is able to produce the fully hydrogenated product (HCOL). On the contrary, in the Pt-WO$_x$/C(550)_sol and Pt-WO$_x$/C(400)_sol, the values of chain carbon atoms differed the one from the other, showing a higher interaction of the C=C double bond rather than the C=O, thus resulting in the higher selectivity toward C=C then C=O.

References

1. Luneau, M.; Lim, J.S.; Patel, D.A.; Sykes, E.C.H.; Friend, C.M.; Sautet, P. Guidelines to Achieving High Selectivity for the Hydrogenation of α,β-Unsaturated Aldehydes with Bimetallic and Dilute Alloy Catalysts: A Review. *Chem. Rev.* **2020**, *120*, 12834–12872.

2. Laref, S.; Delbecq, F.; Loffreda, D. Theoretical elucidation of the selectivity changes for the hydrogenation of unsaturated aldehydes on Pt(111). *J. Catal.* **2009**, *265*, 35–42.

3. Delbecq, F.; Sautet, P. Competitive C=C and C=O adsorption of $α$-$β$ unsaturated aldehydes on Pt and Pd surfaces in relation with the selectivity of hydrogenation reactions :

a theoretical approach. *J. Catal.* **1995**, *152*, 217–236.

4.   Zaera, F. The Surface Chemistry of Metal-Based Hydrogenation Catalysis. *ACS Catal.* **2017**, *7*, 4947–4967.

5.   GALLEZOT, P.; RICHARD, D. Selective Hydrogenation of α,β-Unsaturated Aldehydes. *Catal. Rev.* **1998**, *40*, 81–126.

6.   Mäki-Arvela, P.; Hájek, J.; Salmi, T.; Murzin, D.Y. Chemoselective hydrogenation of carbonyl compounds over heterogeneous catalysts. *Appl. Catal. A Gen.* **2005**, *292*, 1–49.

7.   Cattaneo, S.; Freakley, S.J.; Morgan, D.J.; Sankar, M.; Dimitratos, N.; Hutchings, G.J. Cinnamaldehyde hydrogenation using Au-Pd catalysts prepared by sol immobilisation. *Catal. Sci. Technol.* **2018**, *8*, 1677–1685.

8.   Delbecq, F.; Sautet, P. Competitive C☐C and C☐O Adsorption of α-β-Unsaturated Aldehydes on Pt and Pd Surfaces in Relation with the Selectivity of Hydrogenation Reactions: A Theoretical Approach. *J. Catal.* **1995**, *152*, 217–236.

9.   Tseung, A.C.C.; Chen, K.Y. Hydrogen spill-over effect on Pt/WO3 anode catalysts. *Catal. Today* **1997**, *38*, 439–443.

10.   Tian, Z.; Li, Q.; Hou, J.; Pei, L.; Li, Y.; Ai, S. Platinum nanocrystals supported on CoAl mixed metal oxide nanosheets derived from layered double hydroxides as catalysts for selective hydrogenation of cinnamaldehyde. *J. Catal.* **2015**, *331*, 193–202.

11.   Li, Z.; Yu, R.; Huang, J.; Shi, Y.; Zhang, D.; Zhong, X.; Wang, D.; Wu, Y.; Li, Y. Platinum–nickel frame within metal-organic framework fabricated in situ for hydrogen enrichment and molecular sieving. *Nat. Commun.* **2015**, *6*, 8248.

12.   Zhang, J.; Gao, Z.; Wang, S.; Wang, G.; Gao, X.; Zhang, B.; Xing, S.; Zhao, S.; Qin, Y. Origin of synergistic effects in bicomponent cobalt oxide-platinum catalysts for selective hydrogenation reaction. *Nat. Commun.* **2019**, *10*, 4166.

13.   Kahsar, K.R.; Schwartz, D.K.; Medlin, J.W. Control of Metal Catalyst Selectivity through Specific Noncovalent Molecular Interactions. *J. Am. Chem. Soc.* **2014**, *136*, 520–526.

14.   Dai, Y.; Gao, X.; Chu, X.; Jiang, C.; Yao, Y.; Guo, Z.; Zhou, C.; Wang, C.; Wang, H.; Yang, Y. On the role of water in selective hydrogenation of cinnamaldehyde to cinnamyl alcohol on PtFe catalysts. *J. Catal.* **2018**, *364*, 192–203.

15.   Coq, B.; Figueras, F. Structure–activity relationships in catalysis by metals: some aspects of particle size, bimetallic and supports effects. *Coord. Chem. Rev.* **1998**, *178–180*, 1753–1783.

16. Hu, Q.; Wang, S.; Gao, Z.; Li, Y.; Zhang, Q.; Xiang, Q.; Qin, Y. The precise decoration of Pt nanoparticles with Fe oxide by atomic layer deposition for the selective hydrogenation of cinnamaldehyde. *Appl. Catal. B Environ.* **2017**, *218*, 591–599.

17. Hoang-Van, C.; Zegaoui, O. Studies of high surface area Pt/MoO3 and Pt/WO3 catalysts for selective hydrogenation reactions. II. Reactions of acrolein and allyl alcohol. *Appl. Catal. A Gen.* **1997**, *164*, 91–103.

18. Zhou, W.; Soultanidis, N.; Xu, H.; Wong, M.S.; Neurock, M.; Kiely, C.J.; Wachs, I.E. Nature of Catalytically Active Sites in the Supported WO3/ZrO2 Solid Acid System: A Current Perspective. *ACS Catal.* **2017**, *7*, 2181–2198.

19. Bhanuchander, P.; Samudrala, S.P.; Putrakumar, B.; Vijayanand, P.; Kumar, B.S.; Chary, K.V.R. Hydrogenation of levulinic acid to valeric acid over platinum-tungsten catalysts supported on γ-Al2O3. *New J. Chem.* **2019**, *43*, 18003–18011.

20. Stucchi, M.; Vasile, F.; Cattaneo, S.; Villa, A.; Chieregato, A.; Vandegehuchte, B.D.; Prati, L. An Insight into the Role of Reactant Structure Effect in Pd / C Catalysed Aldehyde Hydrogenation. **2022**.

21. D'Agostino, C.; Brett, G.L.; Miedziak, P.J.; Knight, D.W.; Hutchings, G.J.; Gladden, L.F.; Mantle, M.D. Understanding the Solvent Effect on the Catalytic Oxidation of 1,4-Butanediol in Methanol over Au/TiO2 Catalyst: NMR Diffusion and Relaxation Studies. *Chem. – A Eur. J.* **2012**, *18*, 14426–14433.

22. D'Agostino, C.; Mitchell, J.; Mantle, M.D.; Gladden, L.F. Interpretation of NMR relaxation as a tool for characterising the adsorption strength of liquids inside porous materials. *Chem. - A Eur. J.* **2014**, *20*, 13009–13015.

23. D'Agostino, C.; Feaviour, M.R.; Brett, G.L.; Mitchell, J.; York, A.P.E.; Hutchings, G.J.; Mantle, M.D.; Gladden, L.F. Solvent inhibition in the liquid-phase catalytic oxidation of 1,4-butanediol: understanding the catalyst behaviour from NMR relaxation time measurements. *Catal. Sci. Technol.* **2016**, *6*, 7896–7901.

24. Weber, D.; Mitchell, J.; Mcgregor, J.; Gladden, L.F. Comparing strengths of surface interactions for reactants and solvents in porous catalysts using Two-dimensional NMR relaxation correlations. *J. Phys. Chem. C* **2009**, *113*, 6610–6615.

25. Supothina, S.; Seeharaj, P.; Yoriya, S.; Sriyudthsak, M. Synthesis of tungsten oxide nanoparticles by acid precipitation method. *Ceram. Int.* **2007**, *33*, 931–936.

26. Shim, W.G.; Lee, J.W.; Moon, H. Adsorption of carbon tetrachloride and chloroform on activated carbon at (300.15, 310.15, 320.15, and 330.15) K. *J. Chem. Eng. Data* **2003**, *48*,

286–290.

27.   Zhang, D.-Y.; Ma, Z.-F.; Wang, G.; Chen, J.; Wallace, G.C.; Liu, H.-K. Preparation of Low Loading Pt/C Catalyst by Carbon Xerogel Method for Ethanol Electrooxidation. *Catal. Letters* **2008**, *122*, 111–114.

28.   Yadav, A.K.; Gour, K.S.; Singh, V.N.; Dudeja, S.; Verma, M. *Growth of WO3 nanoparticle for gas sensing applications*; CSIR-National Physical Laboratory: India, 2017;

29.   Venu, R.; Ramulu, T.S.; Anandakumar, S.; Rani, V.S.; Kim, C.G. Bio-directed synthesis of platinum nanoparticles using aqueous honey solutions and their catalytic applications. *Colloids Surfaces A Physicochem. Eng. Asp.* **2011**, *384*, 733–738.

30.   Rodríguez-Proenza, C.A.; Palomares-Báez, J.P.; Chávez-Rojo, M.A.; García-Ruiz, A.F.; Azanza-Ricardo, C.L.; Santoveña-Uribe, A.; Luna-Bárcenas, G.; Rodríguez-López, J.L.; Esparza, R. Atomic Surface Segregation and Structural Characterization of PdPt Bimetallic Nanoparticles. *Mater.* 2018, *11*.

31.   Park, J.; Lee, S.; Kim, H.E.; Cho, A.; Kim, S.; Ye, Y.; Han, J.W.; Lee, H.; Jang, J.H.; Lee, J. Investigation of the Support Effect in Atomically Dispersed Pt on WO3−x for Utilization of Pt in the Hydrogen Evolution Reaction. *Angew. Chemie - Int. Ed.* **2019**, *58*, 16038–16042.

32.   Wang, J.; Wang, Z.; Liu, C.-J. Enhanced Activity for CO Oxidation over WO3 Nanolamella Supported Pt Catalyst. *ACS Appl. Mater. Interfaces* **2014**, *6*, 12860–12867.

33.   Song, J.; Huang, Z.-F.; Pan, L.; Zou, J.-J.; Zhang, X.; Wang, L. Oxygen-Deficient Tungsten Oxide as Versatile and Efficient Hydrogenation Catalyst. *ACS Catal.* **2015**, *5*, 6594–6599.

34.   Qu, X.; Hu, Q.; Song, Z.; Sun, Z.; Zhang, B.; Zhong, J.; Cao, X.; Liu, Y.; Zhao, B.; Liu, Z.; et al. Adsorption and desorption mechanisms on graphene oxide nanosheets: Kinetics and tuning. *Innov.* **2021**, *2*, 100137.